Conduction mechanism of nitronyl-nitroxide molecular magnetic compounds

N. Dotti,[1,2] E. Heintze,[2] M. Slota,[1,2] R. Hübner,[2,3] F. Wang,[4] J. Nuss,[3] M. Dressel,[2] and L. Bogani[1,2,*]

[1]*Department of Materials, University of Oxford, 16 Parks Road, Oxford OX1 3PH, United Kingdom*

[2]*1.Physikalisches Institut, Universität Stuttgart, Pfaffenwaldring 57, D-70550 Stuttgart, Germany*

[3]*Max Plank Institute für Festkörperforschung, Heisenbergstraße 1, D-70569 Stuttgart, Germany*

[4]*Polymer and Materials Chemistry, Lund University, Box 124, SE-22100 Lund, Sweden*

(Received 29 May 2015; revised manuscript received 21 December 2015; published 4 April 2016)

We investigate the conduction mechanisms of nitronyl-nitroxide (NIT) molecular radicals, as useful for the creation of nanoscopic molecular spintronic devices, finding that it does not correspond to standard Mott behavior, as previously postulated. We provide a complete investigation using transport measurements, low-energy, sub-THz spectroscopy and introducing differently substituted phenyl appendages. We show that a nontrivial surface-charge-limited regime is present in addition to the standard low-voltage Ohmic conductance. Scaling analysis allows one to determine all the main transport parameters for the compounds and highlights the presence of charge-trapping effects. Comparison among the different compounds shows the relevance of intermolecular stacking between the aromatic ring of the phenyl appendix and the NIT motif in the creation of useful electron transport channels. The importance of intermolecular pathways is further highlighted by electronic structure calculations, which clarify the nature of the electronic channels and their effect on the Mott character of the compounds.

DOI: 10.1103/PhysRevB.93.165201

I. INTRODUCTION

Molecular magnetic materials offer a particularly rich experimental ground [1], where sophisticated effects can be observed with particular clarity and tuned by means of molecular synthetic chemistry [2–7]. They have allowed, for example, the observation of magnetic quantum tunneling [8–11], Berry phase interference [12], and permitted control of the spin degrees of freedom by light [13–20] or via other external stimuli [21–25]. Recent work has highlighted, in particular, the relevance of molecular magnetic materials for spintronics [26]. A new area, described as molecular spintronics [27–34], has arisen where the molecular magnetic properties can be used to tune the transport properties of electronic devices. This approach has different advantages: the chemical tunability of the magnetic molecules allows precise manipulation of the properties of spintronic systems, the electronic channels can be tuned by using rational chemical design, and the created molecules can be integrated into nanoelectronic devices, such as those formed by graphene [35–38] and carbon nanotubes [39–42], or onto functional surfaces [43–47].

In this picture stable organic radicals constitute an appealing class of compounds because they possess unpaired electrons while being completely organic, and they are attracting rapidly increasing attention for molecular spintronics [48–50], switchable devices [51–54], and batteries [55–62]. For all these purposes radicals are now being integrated into functional nanostructures [63–66], where their spin and electric properties can be exploited [67]. Moreover, organic radicals have attracted attention, since the early days of molecular magnetism, as possible constituents for purely organic ferromagnets [68], or for the creation of molecular magnetic coordination compounds [69–74], including single-molecule magnets and single-chain magnets [69]. The study of the conduction mechanisms in bulk radicals is thus important as a comparison for nanostructured systems and for future investigations on radical-based molecular spintronics.

Electrically, organic radicals are usually classified as Mott insulators [75] because of the strong on-site Coulomb repulsions that hinder charge transport, despite the presence of singly occupied molecular orbitals. At the same time, in-depth investigations have shown the presence of several intermolecular interaction channels, sometimes strong enough to transmit very sizable magnetic interactions [76]. As the magnetic interaction is mediated by the electronic states of the molecules, these channels could, in principle, also be used to facilitate electronic transport in the material. Other transport channels, such as space-charge-limited (SCL) currents [77–80], could become relevant for the conduction of such systems, and the possible presence of charge traps [81–84] also remains to be clarified. The identification of these elements and the possible rationalization of the structure-properties relation would be of fundamental importance for the design and development of spintronic nanodevices that rely on radicals.

Here we investigate the conduction properties of molecular radicals of the nitronyl-nitroxide (NIT-R) family [85,86] that contain an aromatic R appendage attached to the NIT group, by a combination of theoretical modeling, very low-energy (sub-THz) and high-voltage transport measurements. We show that the systems do not follow the standard Mott behavior considered so far and present characteristic channels that can be tuned chemically and can be exploited in prospective nanoscale devices.

II. EXPERIMENTAL METHODOLOGY

We chose to investigate a family of NIT-R radicals containing different aromatic -R groups, with the NIT moiety possessing also oxidized and reduced forms that are stable at room temperature [85] [Figs. 1(a) and 1(b)]. NIT-R radicals contain a single spin center delocalized over two N-O groups and the carbon atom in between, which also links to the

*Corresponding author: lapo.bogani@materials.ox.ac.uk

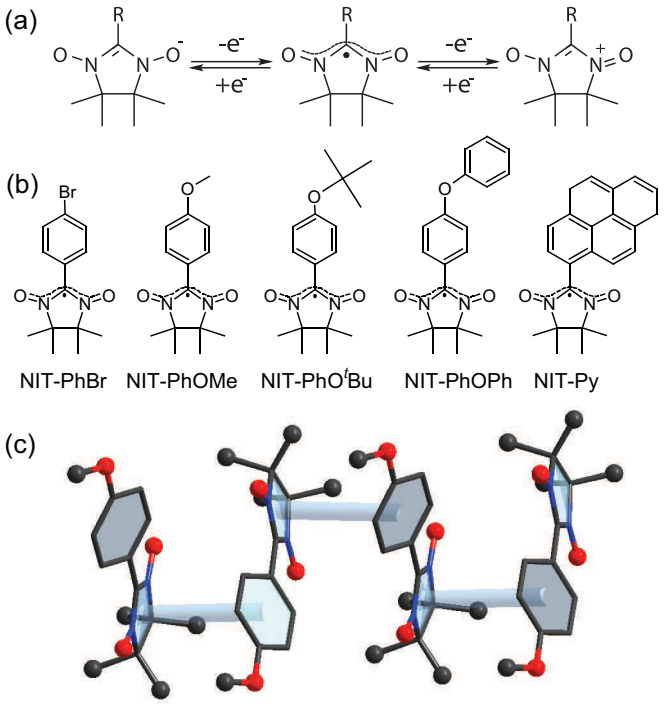

FIG. 1. (a) Schematic representation of the general structure of the nitronyl-nitroxide (NIT-R) radicals, showing the different oxidation states that are available at room temperature and the reduction or oxidation processes from the pristine neutral form. (b) Schematic representation of the five radicals investigated, with the corresponding acronyms below. (c) Crystal structure of radical NIT-PhOMe, with the cylinders highlighting the presence of overlap between the electronic clouds of aromatic appendages and the NIT moiety. Carbon is represented in black, oxygen in red, nitrogen in blue, and hydrogen atoms are omitted for the sake of clarity.

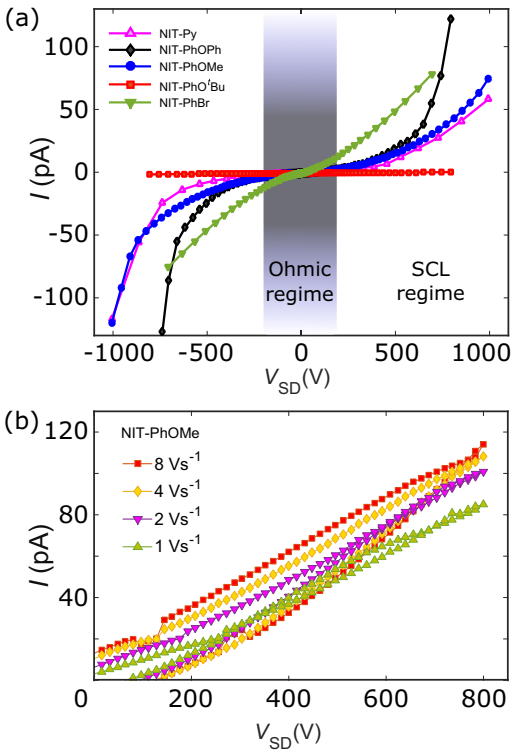

FIG. 2. (a) Room temperature I-V_{sd} characteristic curves resulting from averaging on multiple sets of measurements collected on NIT-PhBr (green down triangles), NIT-PhOMe (blue circles), NIT-PhOtBu (red squares), NIT-PhOPh (black diamonds), and NIT-Py (violet up triangles). (b) Dependence of the I vs V_{sd} curves on the sweep rate of the bias voltage, as acquired for the NIT-PhOMe radical. Decreasing the sweep rate capacitive effects can be minimized, as can be seen from the narrowing gap between forward and backward sweeps and decreased zero-voltage residual current.

peripheral -R functionality. They were chosen because they are interesting for organic switches and produced electronic devices with both p and n behaviors [87,88]. Combined with tetrathiafulvalene moieties, they also showed conductive behavior sensitive to the external magnetic field [89]. The materials that we investigate here have a more insulating character than the tetrathiafulvalene-based compounds and can thus be integrated into memristive and neuromorphic logic devices.

We can then tune the packing of the molecules by using different -R groups. In this way we obtain radicals with different levels of bulkiness and aromaticity, and all radicals investigated are shown in Fig. 1(b). This is particularly appealing to create electronic channels in the material, such as the one reported in Fig. 1(c) for NIT-PhOMe.

All syntheses were performed as described in the Supplemental Material [90]. Briefly, the NIT-R were prepared according to published methods [91,92] and, after purification via column chromatography and recrystallization, single crystals suitable for x-ray diffraction were obtained. The structural data are reported in the Supplemental Material [90] and show the presence of a variety of intermolecular channels, as useful for the purposes of the present investigation. No incorporation of solvents in the structure was ever observed.

The transport characteristics were measured using a two-point-probe setup and were always repeated for several crystals of each compound, so as to ensure the reproducibility and check the variability among different crystal qualities and batches (see Table III and Supplemental Material [90] for details). The typical observed characteristics are reported in Fig. 2(a) for crystals of all NIT-R compounds. All curves clearly show a linear and a nonlinear response at low and high voltages, respectively. Both regimes are roughly symmetrically placed around zero voltage, with the residual asymmetries being attributable to nonperfect contacts. The linear response observed at low voltages in all curves can be assigned to Ohmic behavior, with measured resistances that fall in the tens of TΩ range, about 6 orders of magnitude higher than in tetrathiafulvalene-based NIT-R derivatives [89]. At higher voltages, in the nonlinear region, resistances are in the 1–0.1 TΩ range, indicating the presence of different, less conventional transport channels.

The use of different sweep rates for the source-drain voltage leads to a hysteretic behavior for the fastest sweep rates, as often observed in organic semiconductors [93], that produce devices with high capacitances. Such effects can be minimized by decreasing the sweep rate, as shown in Fig. 2(b), where we plot the dependence of the I vs V_{sd} curves on the voltage sweep

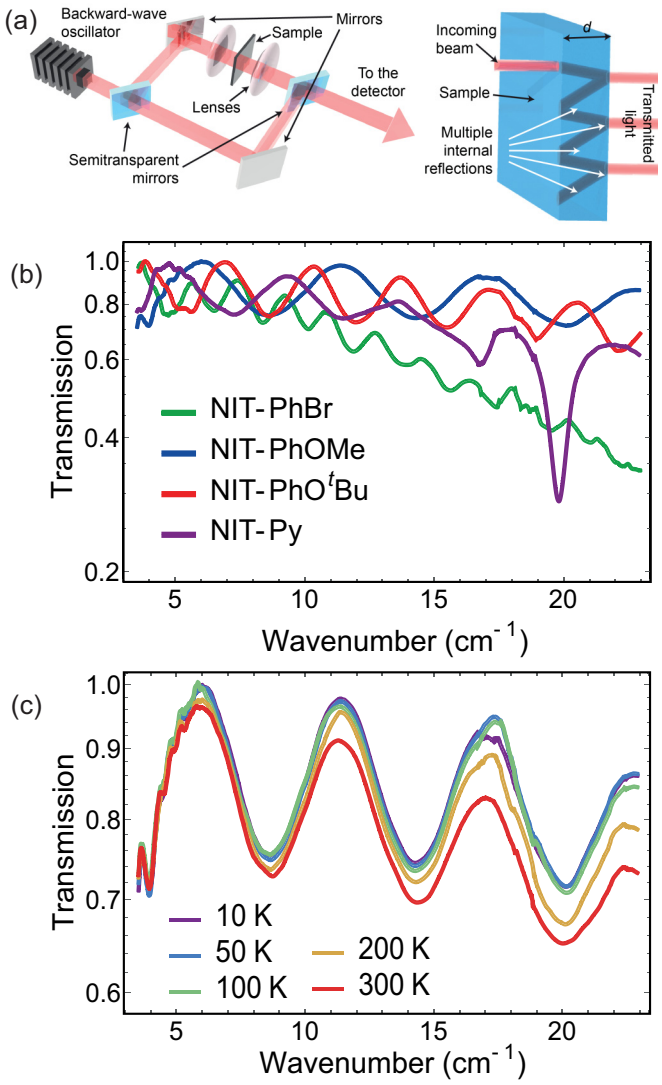

FIG. 3. (a) Scheme of the THz spectrometer used for the measurements (left) and scheme of the multiple internal reflections within the sample, leading to Fabry-Perot interferences (right). (b) Transmission spectra in the 3–23 cm^{-1} range, as measured for the NIT-R compounds on pellets at T=10 K. (c) Temperature and frequency dependence of the transmission spectra of NIT-PhOMe in the 3–23 cm^{-1} and 10–300 K ranges. A vertical logarithmic scale is used for clarity.

rate of V_{sd}. In all the following measurements such capacitive effects were minimized by sweeping V_{sd} slower than 0.2 V/s.

Very low-energy sub-THz spectroscopy is a powerful tool to investigate the electronic properties of low-conducting materials and affords an excellent way to extract the dielectric constant and information on the minimum mobility, $\mu_{\min}$ (see Sec. III). In this technique, depicted in Fig. 3(a), the surfaces of the pellets act as the mirrors of a Fabry-Pérot resonator so that interference effects produced by multiple reflections at the boundaries lead to an alternating transmission that depends on the wavelength, the sample thickness, and the complex refractive index of the compound itself [94]. In this low-energy range of the spectrum, the real part of the optical dielectric constant ϵ_1 coincides with the dc relative permittivity of the material [i.e., ϵ_r in Eq. (2) below] and valuable information on the conduction processes can be obtained [95,96]. Assuming, as commonly done, that the frequency ω dependence of the dielectric constants is negligible, we obtain the ϵ_1 and ϵ_2 values shown in Table I.

TABLE I. Values of ϵ_1 and ϵ_2 as extracted from sub-THz measurements for the NIT-R radicals. ϵ_1 values are obtained by averaging between 2 and 300 K, while the ϵ_2 ones refer to 250 K (see text).

NIT-R	ϵ_1	ϵ_2
NIT-PhBr	2.9 ± 0.2	$6.7 \pm 0.2 \times 10^{-2}$
NIT-PhOMe	2.8 ± 0.1	$2.9 \pm 0.2 \times 10^{-2}$
NIT-PhOtBu	2.79 ± 0.06	$3.95 \pm 0.05 \times 10^{-2}$
NIT-Py	2.61 ± 0.07	$8.18 \pm 0.05 \times 10^{-2}$

The transmission spectra for the analyzed compounds [Fig. 3(b)], as obtained at a temperature of 10 K by dividing the spectrum of the pellet by that of the sources (acquired at exactly the same conditions), contain a superposition of two oscillations. The spectra are devoid of absorptions, except for the NIT-Py radical that shows a vibronic excitation at 20 cm^{-1}. Contrary to expectations for a Mott insulator, the overall transmission decreases with increasing wave number owing to the nonvanishing value of ϵ_2 (Table I). This is another hint for different transport channels within these compounds, and this aspect will be further discussed in Sec. IV. The different transmittivities observed are to be ascribed to different ϵ_2 values and pellet thicknesses.

The temperature T and ω dependences of the response of the radicals always show two regions [see Fig. 3(c) for the behavior of NIT-PhOMe, taken as a typical example]: a low-T region (from 5 to 50 K), where no temperature evolution of the absorption is observed, and a $T > 50$ K region, where the transmission signal decreases with increasing T. We observe that ϵ_2 is always relatively small, with a clear increase upon increasing T due to the higher out-of-phase response of thermally generated free charge carriers. On the contrary, ϵ_1 shows no T dependence within our experimental error and varies for the different NIT-R radicals between 2.6 and 3 (Table I). All NIT-R compounds show roughly the same ϵ_1 value, often within our experimental error, and this defines the range of values to be typically expected for such materials.

III. EXTRACTION OF THE TRANSPORT PARAMETERS

For each system we can define a threshold voltage V_c between the Ohmic regime and the nonlinear regime (Table II). Below V_c the density of thermally generated free carriers inside the crystal is dominant with respect to the injected charge carriers. The behavior is hence given by Ohm's law, which, neglecting diffusive contributions to the current, provides the current density:

$$J_\Omega = \frac{I_\Omega}{W} = e n_{\rm th} \mu_0 \frac{V_\Omega}{L}, \quad (1)$$

where the subscript Ω denotes the Ohmic regime, e is the electron charge, $n_{\rm th}$ is the thermal-equilibrium carrier density, W and L are the width and the length of the electronic

TABLE II. Minimum mobility $\mu_{\min}$, surface thermal carrier density n_{th}, sheet resistance R_S, crossover voltage V_c, Ohmic conductance and fitting exponent (G_Ω and η_Ω), charge-limited parameters G_{SCL} and η_{SCL}, and low-field mobility μ_0 for the different NIT-R radicals, as extracted from the optical and transport measurements.

NIT-R	$\mu_{\min}$ [cm^2 V^{-1} s^{-1}]	n_{th}(2D) [10^{13} m^{-2}]	R_S [TΩ]	V_c[a] [V]	G_Ω[a] [fS]	η_Ω[a]	G_{SCL}[a] [fS V$^{\eta-1}$]	η_{SCL}[a]	μ_0 [cm^2 V^{-1} s^{-1}]
NIT-PhBr	$3.0\pm0.5\times10^{-2}$	1.0 ± 0.5	0.9 ± 0.3	40 ± 20	55 ± 10	0.9 ± 0.3	6.3 ± 0.9	1.5 ± 0.1	$6\pm4\times10^{-3}$
NIT-PhOMe[b]	$4\pm3\times10^{-3}$	4.2 ± 0.8	2.2 ± 0.3	170 ± 30	23 ± 3	1.2 ± 0.1	0.9 ± 0.6	1.7 ± 0.1	$7\pm1\times10^{-4}$
NIT-PhO^{t}Bu	$7\pm4\times10^{-4}$	17 ± 2	75 ± 4	510 ± 40	0.89 ± 0.03	0.9 ± 0.3	0.2 ± 0.1	1.5 ± 0.3	$5.0\pm0.5\times10^{-6}$
NIT-PhOPh	$6\pm3\times10^{-3}$	3 ± 1	3 ± 1	130 ± 40	18 ± 8	1.1 ± 0.2	1.2 ± 0.7	2.0 ± 0.3	$7\pm4\times10^{-4}$
NIT-Py	$1.4\pm0.9\times10^{-4}$	0.9 ± 0.4	5 ± 3	60 ± 30	6 ± 3	0.9 ± 0.5	$1\pm0.9\times10^{-2}$	2.1 ± 0.3	$1.4\pm0.9\times10^{-3}$

[a]Errors represent the widths of the statistical distributions.
[b]Values refer to $\epsilon_1 = 2.8 \pm 0.2$, see text.

channel, respectively, and μ_0 the charge-carrier mobility at low electric fields. From the linear regime in the I vs V curves we can then evaluate the sheet resistance $R_S = V_\Omega I_\Omega^{-1} W L^{-1}$, where we take $W = 20\,\mu$m as the tip diameter contacting the crystal and $L = 400\,\mu$m is the distance between the tips for each crystal. For all substituents -R attached to the NIT-R radical, we obtain high R_S values (in the TΩ range, Table II) and this already provides important information on the transport mechanism present in the NIT-R family: the high sheet resistances indicate localized transport processes being dominant over delocalized ones. In order to corroborate this observation, the carrier mobility, which can be derived from the measurements as shown below, is a useful parameter to start distinguishing between the different possible transport mechanisms. The boundary between delocalized and localized transport processes, i.e., between band and hopping transport, is commonly considered at charge-carrier mobilities in the range of 0.1–1 cm^2 V^{-1} s^{-1} [81,84]. For all NIT-Rs, extremely low mobilities in the order of 10^{-3} to 10^{-6} cm^2 V^{-1} s^{-1} are obtained, indicating that intermolecular hopping transport is dominant [Fig. 1(a)].

The nonlinear behavior at high voltages is more intriguing: insulating crystals [97], organic semiconductors (both in crystalline [98] and film [81,83] forms), and even semiconducting nanowires [99–101] may display complex transport phenomena such as space-charge-limited currents [102]. SCL transport arises when the contacts to the electron reservoirs are Ohmic and the material is not a good conductor, so that at high voltages an excess of free carriers is injected into the material in the vicinity of the contact. In this situation, the current through the material is no longer limited by its resistance but by the accumulated space charge, which clogs the conductance channel. As a result, SCL currents allow the investigation of many intrinsic properties of the material that are not easily available in the standard Ohmic regime, such as charge-carrier mobility, thermal-equilibrium carrier concentration, and charge trap densities (Fig. 4). For NIT-Rs, due to both the high resistance of the bulk material and the contact geometry, the systems will follow surface SCL currents rather than bulk SCL [77]. The main characteristic of SCL currents is the presence of a noninjection-limited regime after the Ohmic regime, i.e., above the crossover voltage V_c, where I is proportional to AV^2, with a proportionality constant A that depends on the contact geometry. In our case, where two electric probing tips contact the molecular crystal at the same crystal surface, the relationship for surface SCL currents is [77]

$$I_{SCL} = \frac{2}{\pi}\frac{\mu_{\min}\epsilon_0\epsilon_r W}{L^2}V^2, \tag{2}$$

where ϵ_r is the dielectric constant of the material and $\mu_{\min}$ is the minimum carrier mobility, which includes the contact quality and the presence of traps in the electron channel.

Variations in the contact and channel characteristics can influence the absolute current values in this regime, generating sensible crystal-to-crystal variability. Small curve

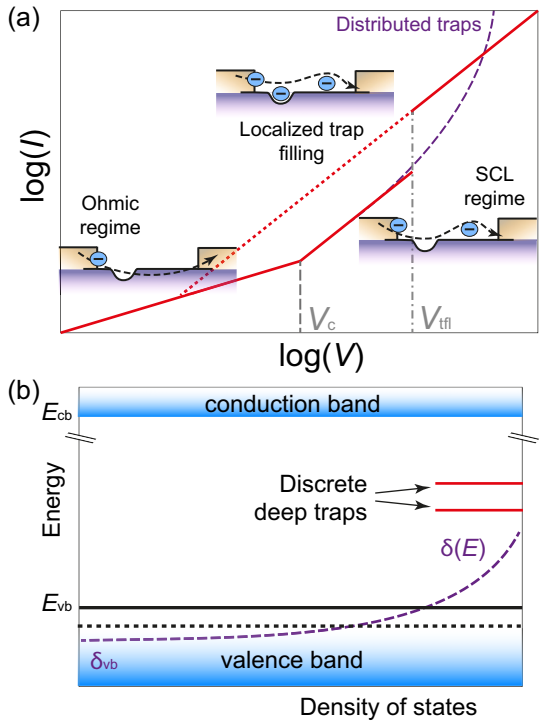

FIG. 4. (a) Schematic representation of the different conduction regimes available for the NIT-R radicals. The Ohmic regime, present at low voltages, gives way, at higher voltages, to surface-charge-limited transport with possible trap effects. The effects of exponentially distributed (violet) and localized-energy (red) traps are also shown. (b) Schematic depiction of the different types of traps available for NIT-R systems, with the localized traps (red lines) and energetically distributed traps (violet curve) placed between the valence and conduction bands of the system.

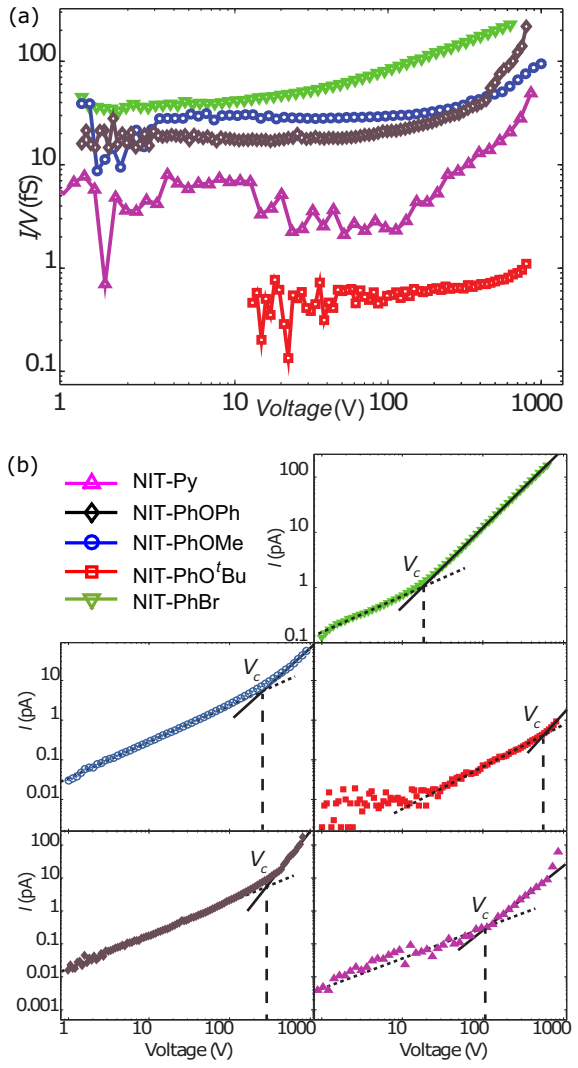

FIG. 5. (a) Bilogarithmic plot of the voltage dependence of the conductance for all NIT-R compounds, showing the constant value for lower voltages, connected to the Ohmic regime, and the raising in conductance at higher voltages, where SCL effects become dominant. (b) Bilogarithmic plots of the current vs source-drain voltage characteristic curves for the different NIT-R compounds. The dashed and continuous lines show the fitting for the Ohmic and SCL regimes, respectively. (See Table II and Fig. 6 for the results.) The crossover voltages V_c, as obtained from the intersection of the two regimes, are also highlighted with vertical lines.

asymmetries for positive and negative voltages are also consistent with these effects and are usually ascribed to different hole and electron trapping potentials. This variability can be taken into account by performing a statistical analysis on the slope of the I versus V curves, which is related to the conduction mechanisms and is independent of the absolute value of the resistivity. A common way to identify the presence of SCL currents is by plotting the linear conductance $G = I/V$ vs V in a log-log plot, which will yield a straight horizontal line for the Ohmic regime, and a sudden increase in conductivity once the SCL regime triggers. All NIT-Rs show this behavior [Fig. 5(a)], whatever R, clearly highlighting the presence of SCL currents.

We can now combine the optical and transport measurements to obtain information on the *minimum mobility* ($\mu_{\min}$) as, at the ω used, the extracted ϵ_1 coincides with ϵ_r in Eq. (2). It should be noticed that all NIT-R show roughly the same ϵ_1 value and that variations much larger than those observed in the series do not introduce important variations in the extracted $\mu_{\min}$. Thus the ϵ_1 of NIT-PhOPh can be safely considered to be, for our purposes, 2.8 ± 0.2. We can thus extract $\mu_{\min}$ for all compounds, using $W = 20$ μm and $L = 400$ μm as before (Table II), and it can be seen that it strongly depends on the radical substituent, with NIT-PhBr exhibiting the highest one, followed by NIT-PhOMe and NIT-PhOPh. Eventually the lowest mobilities belong to NIT-PhOtBu and NIT-Py, which show very similar conductivities, at the limit of our detection range. Information on the conduction mechanisms can be extracted from the voltage threshold V_c between the Ohmic and SCL regimes, where we have $I_\Omega = I_{SCL}$ and thus we can evaluate the thermal-equilibrium carrier density at the crystal surface by

$$n_{\text{th}} = \frac{2}{\pi}\frac{\epsilon_0 \epsilon_r}{e}\frac{V_c}{L}. \tag{3}$$

To extract the threshold voltages we can plot the current in both the Ohmic and the SCL regimes in a double logarithmic plot [Figs. 5(b)–5(f)] and then fit the curves with the function $I = G_i V^\eta$, where the i index stands for the Ohmic ($i = \Omega$) or charge-limited ($i = \text{SCL}$) regions and the exponent η varies between the two regimes. V_c is then obtained from the intercept between the fits of the high- and low-voltage regions. In order to account for the variability among the different sample geometries and measurements, a statistical analysis was performed by acquiring several sets of measurements for each compound on different crystals (see Supplemental Material [90]) and performing the fitting procedures on all of them. [Figure 6(a) shows a small subset of measurements.] The resulting statistical analysis provided a Gaussian distribution for each exponent, as shown in Fig. 6, from which the values provided in Table II were extracted. All compounds with the higher mobilities show a value of the SCL exponent slightly below the predicted value of 2, while the two systems with the lowest conductance and the least efficient intermolecular channels provide exactly 2, within experimental error. These compounds also display a wider dispersion of behaviors, with a few cases showing exponents up to 3. This effect is actually to be linked to a more limited experimental accuracy produced by the presence of other mechanisms, such as traps (see Sec. V), and the limited voltage range between V_C and the breakdown voltage of the crystals. All compounds show an effective thermal carrier density in the order of 10^{13} m^{-2} at the crystal surface, with only a small dependence on the -R group observable, in perfect compatibility with the expected variability in the quality of the crystal-electrode contacts.

IV. MODELING OF THE TRANSPORT

In a pure Mott insulator the main parameter that influences the conductance is the charging energy needed to add an electron to a neutral molecule. For the NIT-R systems the main parameters are the distance between the upper and lower Hubbard bands and the energy distances of the singly

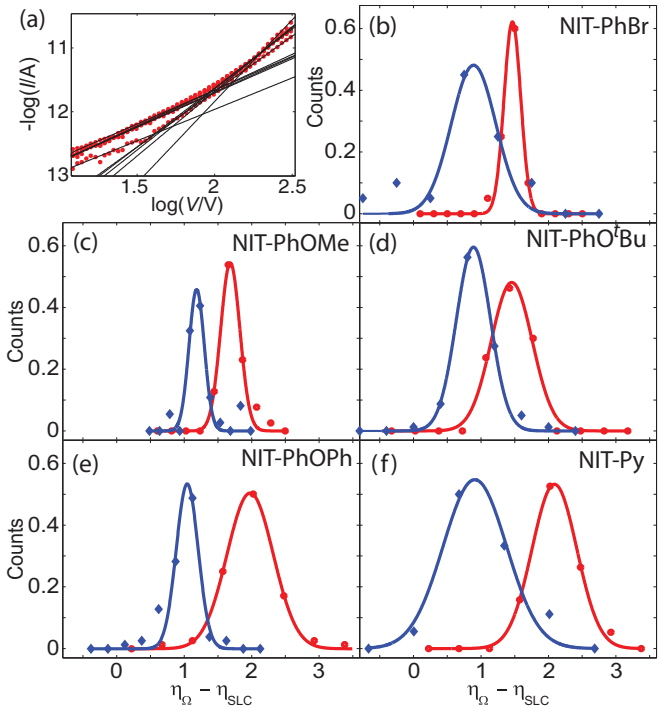

FIG. 6. (a) Example of fitting of the different regimes for a number of measurements performed on NIT-PhOMe, allowing the statistical analysis of the conduction regimes. Details about data sets in Table III. The resulting distribution of the exponents, as obtained for the low-voltage (blue diamonds) and high-voltage (red dots) regimes, are shown in (b) for NIT-PhBr, (c) for NIT-PhOMe, (d) for NIT-PhOtBu, (e) for NIT-PhOPh, and (f) for NIT-Py. No-count points are shown for clarity, and solid lines correspond to Gaussian fits (values in Table II).

occupied molecular orbital (SOMO or α-HOMO) and the lowest unoccupied molecular orbital (LUMO) from the highest occupied molecular orbital (HOMO) [103]. To gain insight into these parameters, we performed numerical calculations with full geometry optimizations of the NIT-Rs carried out using the density functional theory method (DFT) at the B3LYP level [104]. All atoms were assigned a 6-311++G** basis set and calculations were performed with SPARTAN14 program packages [105]. The results (Table IV) show that the energy differences between the three orbitals are identical for all compounds except for NIT-Py, which is only a little

TABLE III. Specifications on the number of measurements used for statistical analysis. Several *I*-*V* cycles were performed on the indicated number of crystals. It should be noticed that each curve contributed four points to our analysis, for forward and backward sweeps at positive and negative voltages.

NIT-R	Total *I*-*V* curves	Number of crystals
NIT-PhBr	15	2
NIT-PhOMe	23	3
NIT-PhO^{t}Bu	27	2
NIT-PhOPh	45	3
NIT-Py	5	1

TABLE IV. Calculated energy distances of the SOMO and LUMO orbitals from the HOMO, crystallographic distances and tilting angles between the aromatic components of adjacent molecules for the different NIT-R compounds.

NIT-R	SOMO [eV]	LUMO [eV]	*r* [Å]	Angle [°]
NIT-PhBr	0.7	3.6	4.760	4.08
NIT-PhOMe	0.4	3.3	4.332	33.23
NIT-PhO^{t}Bu	0.6	3.5	5.911	56.15
NIT-PhOPh	0.5	3.4	N.A.	N.A.
NIT-Py	0.3	3.3	5.895	43.13

higher. This is in good agreement with our estimation of the number of carriers n_{th} (Table II) but is not enough to explain the large conductivity differences, indicating that the main limiting factor is not the molecular charging energy itself, but the intermolecular barrier that has to be overcome for the transport process to occur. As such, barriers are much more sensitive to the molecular arrangement in the bulk and the steric of the -R substituents can thus become an important factor.

Insight on this intermolecular conduction path can be obtained theoretically by DFT calculations on the crystal structure of the NIT-PhOMe system, which has a smaller unit cell compared to the others, containing only four molecular units, and can thus be treated with reasonable computing power. For these electronic structure calculations we employed the Vienna *ab initio* simulation package (VASP) [106–109] using the projector augmented-wave (PAW) pseudopotentials [110] and the Perdew-Burke-Ernzerhof generalized gradient approximation (PBE-GGA) [111].

The energy cutoff for the plane-wave basis set was put at 400 eV, and the first Brillouin zone was sampled with a 7×7×7 Monkhorst-Pack *k*-points mesh [112]. The resulting orbitals, as depicted in real space (Fig. 7, right), show a fragmented

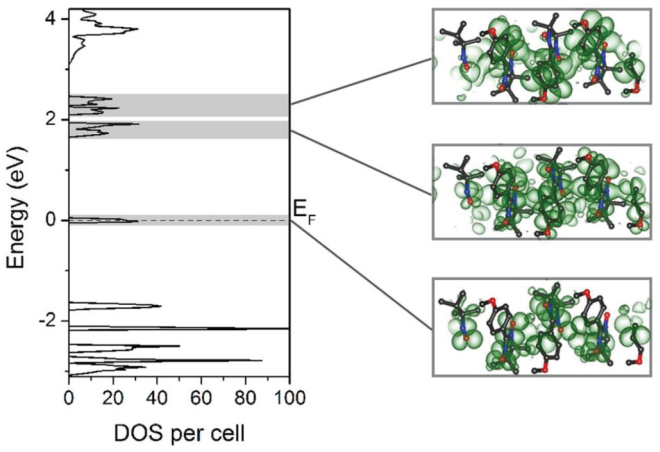

FIG. 7. Left: Calculated DOS for NIT-PhOMe showing the different densities close to E_F and charge density maps obtained by projecting in real space the states in different energy intervals, as highlighted by the shaded areas. Right: Charge density maps obtained for NIT-PhOMe by projecting in real space the states around E_F (bottom panel) and around 2 eV (upper panels).

structure with no clear conduction path. On the contrary, the orbitals above the Fermi energy show a delocalization of the states. Analysis as a function of the strength of the on-site interaction U in a DFT+U approach revealed that no band gap is opened at the Fermi level even for U up to 6 eV. Such levels of interaction did not qualitatively change the density of states of the radicals at all, indicating that the charge transport does not follow the standard mechanisms of a Mott insulator. On the contrary, analysis of the charge density maps, as obtained by projecting in real space all states belonging to specific energy intervals, shows the localized characteristic of the states around E_F and the delocalized conduction channels of the states between 1.5 and 2.5 eV. These numerical results thus support the idea that NIT-Rs do not completely behave as Mott insulators: instead they sport a minor density of states around the Fermi energy, which can be easily filled, so that conduction electrons must then be injected at much higher energies.

We can experimentally verify this hypothesis by varying the intermolecular channel via the different -R groups in the systems. π-stacking interactions between each aromatic phenyl group of the -R appendages and the NIT group of the neighboring molecule, as depicted in Fig. 1(c) for NIT-PhOMe, is found in all compounds but with very considerable differences. Radicals with bulky -R substituents that hinder intermolecular interactions lead to intermolecular distances along the channel and tilting angles (taken between the planes of the phenyl ring and of the five-membered heterocycle of the NIT group) that deviate considerably from the standard π-stacking values (Table IV). We can observe that systems with the larger distances between the stacking aromatic groups display indeed lower conductances. The effect is particularly clear-cut in NIT-PhOtBu and NIT-Py, where the large tilt between the two planes produces a disruption of the stacking pattern and extremely low conductances. These structural trends confirm that the conductance is not simply limited by a Mott mechanism but is assisted by a developed intermolecular electron channel. By applying high voltages we can thus inject electrons into the material which can diffuse through it, exploiting these overlapping channels. It should be noticed that the orbital overlaps we consider here are between neighboring molecules and are not intramolecular ones (Fig. 7, right).

These conclusions are also corroborated by the T dependence of ϵ_2, whose logarithm is reported in Fig. 8. The optical ϵ_2, at low photon frequencies ω, is directly related to the mobility of the carriers μ by the relation $\epsilon_2 = A\mu$ [with the proportionality constant [94] $A = \omega/(4e\pi n_{\rm th})$]. The data do not scale as expected for Mott insulators [90] and can only be reproduced, for all NIT-R, by considering hopping of small polarons [113] in the Holstein model. The low-T minimum, clearly present for all NIT-R, can be understood in the framework of transport theories of electron hopping among molecules assisted by vibrational effects modulating the electronic channel [84,113,114]. According to these models the electron mobility should first decrease, on lowering T, because of the progressive decrease of available vibrational modes that assist the hopping, as indeed observed (Fig. 8) down to $T \approx 30$ K. The analytical form for the

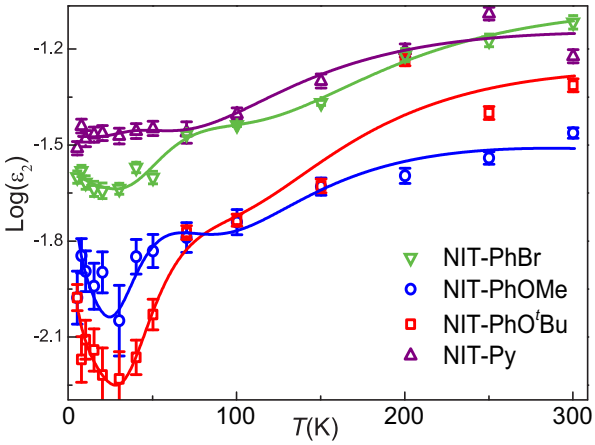

FIG. 8. Temperature dependence of the logarithm of the optical ϵ_2 value for NIT-PhBr (green triangles), NIT-PhOMe (blue dots), NIT-PhOtBu (red squares), and NIT-Py (violet triangles), as determined from the fitting of the sub-THz spectra. Solid lines correspond to fits with the expected behavior for small polarons and low-temperature residual conductivity, as described in the text.

mobility,

$$\mu_{\rm pol} = \frac{\pi^{1/2} e a^2 J^2 e^{-\frac{W_p}{2k_B T}}}{\hbar (2W_p)^{1/2} (k_B T)^{3/2}}, \tag{4}$$

relies on the lattice constant a of the crystal in which the small polaron occurs, the polaron interaction potential J, and the thermal activation energy for hopping W_p, given by half the small-polaron binding energy. All the extracted polaron energies are in the order of 0.4 eV, about the magnitude of the HOMO-SOMO distance, and are comparable to the energies expected from the DFT calculations to reach the delocalized electron channel, confirming, again, the relevance of this non-Mott-like intermolecular channel.

Below 30 K an increase of ϵ_2 is typically observed. This cannot be accounted for by simple hopping, and such observations are typically ascribed to the effects of polaron tunneling and residual bandlike conductivity, again in agreement with the aforementioned DFT calculations. To account for these effects we can add two terms to Eq. (4), accounting for the tunneling and the bandlike conductance:

$$\mu_{LT} = \mu_{\rm tun} + \mu_{BL} = \frac{e a^2}{\hbar \gamma k_B T} \left[\frac{\gamma}{\pi} \xi \right]^{\frac{1}{2}} e^{(-2\gamma\xi)} + dT^{-n}, \tag{5}$$

where $\xi = \mathrm{csch}(\frac{W_p}{2\gamma k_B T})$, γ is a measure of the strength of the electron phonon coupling, and n is an empirical exponential describing the bandlike processes. The expression reproduces well all curves for all NIT-R radicals down to 2 K, and the γ term is always found to be between 2 and 3, which still indicates a relatively weak electron-phonon coupling, even though higher than many organic semiconductors. In all cases we could not reproduce the data with the tunneling term $\mu_{\rm tun}$ alone without including the power-law dependence of μ_{BL}. This confirms again the very important role of the intermolecular interaction channels.

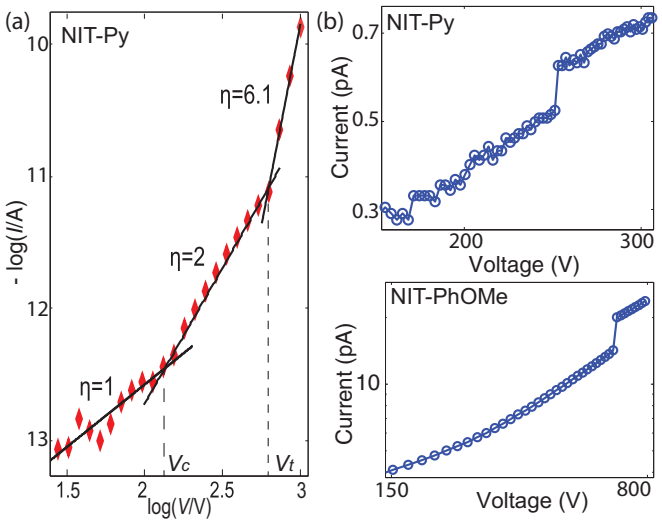

FIG. 9. (a) Example of the presence of distributed traps within the SOMO-LUMO gap, as observed on a bilogarithmic plot. The black lines represent the exponents that indicate the conductivity regime of each part of the curve. Over $V_t = 500$ V the effect of distributed traps is clearly visible, as explained in the text. (b) Examples of localized traps for NIT-Py (top) and NIT-PhOMe (bottom).

V. TRAP EFFECTS

Trap states and additional conduction paths can become relevant at higher voltages [115,116]. Figure 9 shows examples of the very appreciable deviations from the purely quadratic I vs V dependence that can be observed. Both experiments [81] and theory [117,118] indicate that surface traps can strongly influence the SCL regime of molecular crystals, with traps often created at the crystal-contact interface and at defective molecular sites. In the present case we can identify two main trapping mechanisms (Fig. 9). The first type of trap produces an exponential distribution of trap states below the LUMO, described by [119] $\rho_t(E) = (\delta_t/E_t)\exp(E/E_t)$, where δ_t is the trap density, E_t the characteristic trap depth, and E the energy relative to the conduction or valence band. These traps are gradually filled, leading to a current that increases faster than quadratic following the expression [119]

$$I \propto V^{m+1}/d^{2m+1}, \tag{6}$$

where m is given by $m = E_t/k_BT > 1$ and d is the thickness of the sample. As the resulting current only depends on the trap depth but is independent of the device geometry, a power-law dependence of the I vs V characteristics with such a behavior can be regarded as an indication for trap-limited SCL processes. Exponentially distributed traps can explain the deviations from the quadratic I vs V behavior wherever $\eta > 2$ is observed, as, for example, in NIT-Py in Fig. 9. Anyway, the NIT-R systems show far better agreement with the ideal SCL regime than most other molecular conductors, possibly due to the low energy of the traps and the surface SCL mechanism: for example, in AlQ_3, values of $6 < m < 10$ have been found, with trap energies $E_t = 0.15$ eV [120,121]. As the present theoretical background for distributed traps considers neither hopping transport nor surface conductance [122], the behavior is best modeled by introducing a field-dependent mobility, without considering a theoretically derived distribution of traps and characteristic temperatures, as already employed for AlQ_3 and PPV devices [123,124]. We can then assume the mobility to depend on the electric field E via the Poole-Frenkel mechanism [117]:

$$\mu(E) = \mu_0 \exp\left(\frac{e^{3/2}}{k_BT}\sqrt{\frac{E}{\pi\epsilon_0\epsilon_r}}\right), \tag{7}$$

where μ_0 is the low-field mobility [81]. With the previously extracted thermal charge-carrier density we can so calculate μ_0 with Eq. (1) and substitute $\mu_{\min}$ by the Poole-Frenkel mobility $\mu(E)$ in Eq. (7). The resulting I vs V dependence can be used to describe the superquadratic behavior at higher voltages that some of the compounds show [see Fig. 9(a)]. Higher distributed trap densities in the proximity of the electrodes are likely responsible for the underestimated currents close to V_c and any remaining sweep-rate-independent discrepancies between the forward and backward sweeps (Fig. 2).

The second kind of traps that can be observed are localized electron traps, energetically located deep in the band gap of the material [81]. In NIT-R systems these traps can take the form of locally altered molecules, oxidized, or reduced single molecules or chemically defective regions, which can arise, for example, by the presence of the amino-nitroxide side product radical in the crystalline NIT-R. Two examples of such traps are shown in Fig. 9(b), with clear signatures of vertical jumps at the so-called trap-filling voltage V_{TFL}, above which transport is in the so-called trap-filled limit and continues to follow the quadratic voltage dependence. In the case of surface SCL currents, traps are filled by the injected charge at

$$V_{TFL} = \frac{\pi}{4\epsilon_0\epsilon_r} eL\delta_d, \tag{8}$$

from which the trap density per unit surface area δ_d can be evaluated. (The subscript d denotes deep traps, located at several times k_BT from the valence band.) This is also visible from the current jumps due to trap filling, which would be absent for a dense distribution of traps close to the conduction band. The presence of such deep traps, which are typically filled close to 0.4 eV, is typical of systems with very wide band gaps and would match with a gap width close to the 3 eV, as previously discussed. The observed densities of localized traps are ca. $\delta_d = 3.5 \pm 0.3 \times 10^{10}$ cm^2, which agrees with known densities in organic conductors [125–129] and, in particular, to those of rubrene crystals [130].

VI. CONCLUSIONS

In conclusion, we have shown that, contrary to what has been conjectured until now, the widespread compounds of the NIT-R class do not behave as typical Mott insulators when -R is aromatic, owing to interactions between the π electronic cloud of the phenyl appendix and the delocalized NIT motif. These results are fundamental for the creation of spintronic nanodevices based on NIT-R radicals and allow use of chemical design to tune the conduction properties of these materials. The space-charge limited currents and strong trap effects here evidenced will be fundamental for the design of any nanoscale devices based on such materials, and in

particular for latch memory, field-effect, and spintronic devices [131–138]. The observed mobilities fall in the correct range for the creation of memristive devices, where charge-limiting effects can be desirable to create nanometer-scale logic units. Such effects, which have until now been ignored, will thus be of fundamental importance for proposed molecular switching devices [13] at the nanoscale.

In this paper we have also set a methodological standard for the investigation of the conduction regimes of low-conductive magnetic compounds [96] by providing a combination of optical measurements at sub-THz frequencies, transport data, and numerical calculations. The results will constitute the experimental and theoretical backbone for the study of electron transport in NIT-R-based complexes [96], which are attracting particular interest for their slow-relaxing behavior [69] and the possibility of controlling them with light [13].

ACKNOWLEDGMENTS

We acknowledge financial support from the Baden-Württemberg Stiftung (Kompetenznetz Funktionelle Nanostrukturen), the Alexander von Humboldt Stiftung (Sofja Kovalevskaja Award), the European Research Council (ERC-StG 338258 "OptoQMol"), and the Royal Society via a University Research Fellowship and URF Grant.

[1] D. Gatteschi, R. Sessoli, and J. Villain, *Molecular Nanomagnets* (Oxford University Press, Oxford, UK, 2006).
[2] G. E. Kostakis, I. J. Hewitt, A. M. Ako, V. Mereacre, and A. K. Powell, Philos. Trans. R. Soc., A **368**, 1509 (2010).
[3] R. W. Saalfrank, H. Maid, and A. Scheurer, Angew. Chem., Int. Ed. Engl. **47**, 8794 (2008).
[4] A. Mandel, W. Schmitt, T. G. Womack, R. Bhalla, R. K. Henderson, S. L. Heath, and A. K. Powell, Coord. Chem. Rev. **190–192**, 1067 (1999).
[5] D. N. Woodruff, R. E. P. Winpenny, and R. A. Layfield, Chem. Rev. **113**, 5110 (2013).
[6] K. S. Pedersen, J. Bendix, and R. Clrac, Chem. Commun. (Cambridge, UK) **50**, 4396 (2014).
[7] *Single-Molecule Magnets and Related Phenomena*, edited by R. Winpenny (Springer-Verlag, Berlin, Heidelberg, 2006), Vol. 112.
[8] D. Gatteschi and R. Sessoli, Angew. Chem., Int. Ed. Engl. **42**, 268 (2003).
[9] B. Barbara, L. Thomas, F. Lionti, I. Chiorescu, and A. Sulpice, J. Magn. Magn. Mater. **200**, 167 (1999).
[10] L. Gunther and B. Barbara, *Quantum Tunneling of Magnetization-QTM94: Proceedings of the NATO Advanced Research Workshop, Grenoble and Chichilianne, France* (Kluwer Academic Publishers, Dordrecht, 1995).
[11] J. R. Friedman, M. P. Sarachik, J. Tejada, and R. Ziolo, Phys. Rev. Lett. **76**, 3830 (1996).
[12] W. Wernsdorfer and R. Sessoli, Science **284**, 133 (1999).
[13] E. Heintze, F. El Hallak, C. Clauß, A. Rettori, M. G. Pini, F. Totti, M. Dressel, and L. Bogani, Nat. Mater. **12**, 202 (2013).
[14] M. Slota, M. Blankenhorn, E. Heintze, M. Vu, R. Hübner, and L. Bogani, Faraday Discuss. **185**, 347 (2015).
[15] O. Sato, J. Tao, and Y.-Z. Zhang, Angew. Chem., Int. Ed. Engl. **46**, 2152 (2007).
[16] D. Pinkowicz, M. Ren, L.-M. Zheng, S. Sato, M. Hasegawa, M. Morimoto, M. Irie, B. K. Breedlove, G. Cosquer, K. Katoh, and M. Yamashita, Chemistry **20**, 12502 (2014).
[17] M. Verdaguer, Science **272**, 698 (1996).
[18] O. Sato, T. Iyoda, A. Fujishima, and K. Hashimoto, Science **272**, 704 (1996).
[19] T. Liu, H. Zheng, S. Kang, Y. Shiota, S. Hayami, M. Mito, O. Sato, K. Yoshizawa, S. Kanegawa, and C. Duan, Nat. Commun. **4**, 2826 (2013).
[20] S. Ohkoshi, S. Takano, K. Imoto, M. Yoshikiyo, A. Namai, and H. Tokoro, Nat. Photon. **8**, 65 (2013).
[21] A. S. Zyazin, J. W. G. van den Berg, E. A. Osorio, H. S. J. van der Zant, N. P. Konstantinidis, M. Leijnse, M. R. Wegewijs, F. May, W. Hofstetter, C. Danieli, and A. Cornia, Nano Lett. **10**, 3307 (2010).
[22] M. Trif, F. Troiani, D. Stepanenko, and D. Loss, Phys. Rev. Lett. **101**, 217201 (2008).
[23] O. Sato, T. Kawakami, M. Kimura, S. Hishiya, S. Kubo, and Y. Einaga, J. Am. Chem. Soc. **126**, 13176 (2004).
[24] S.-I. Ohkoshi, K.-I. Arai, Y. Sato, and K. Hashimoto, Nat. Mater. **3**, 857 (2004).
[25] S. Margadonna, K. Prassides, and A. N. Fitch, Angew. Chem., Int. Ed. Engl. **43**, 6316 (2004).
[26] S. Maekawa, *Concepts in Spin Electronics* (Oxford University Press, Oxford, UK, 2006), Vol. 13.
[27] J. Park, A. N. Pasupathy, J. I. Goldsmith, C. Chang, Y. Yaish, J. R. Petta, M. Rinkoski, J. P. Sethna, H. D. Abruña, P. L. McEuen, and D. C. Ralph, Nature (London) **417**, 722 (2002).
[28] D. Rugar, R. Budakian, H. J. Mamin, and B. W. Chui, Nature (London) **430**, 329 (2004).
[29] R. Vincent, S. Klyatskaya, M. Ruben, W. Wernsdorfer, and F. Balestro, Nature (London) **488**, 357 (2012).
[30] A. Saraiva-Souza, M. Smeu, L. Zhang, A. G. Souza Filho, H. Guo, and M. A. Ratner, J. Am. Chem. Soc. **136**, 15065 (2014).
[31] S. Sanvito, Chem. Soc. Rev. **40**, 3336 (2011).
[32] A. R. Rocha, V. M. García-Suárez, S. W. Bailey, C. J. Lambert, J. Ferrer, and S. Sanvito, Nat. Mater. **4**, 335 (2005).
[33] L. Bogani and W. Wernsdorfer, Nat. Mater. **7**, 179 (2008).
[34] S. Jiang, K. Go, C. Cervetti, and L. Bogani, Sci. China: Chem. **55**, 867 (2012).
[35] J. Choi, H. Lee, K. J. Kim, B. Kim, and S. Kim, J. Phys. Chem. Lett. **1**, 505 (2010).
[36] S. Bhandary, S. Ghosh, H. Herper, H. Wende, O. Eriksson, and B. Sanyal, Phys. Rev. Lett. **107**, 257202 (2011).
[37] A. Candini, S. Klyatskaya, M. Ruben, W. Wernsdorfer, and M. Affronte, Nano Lett. **11**, 2634 (2011).
[38] H. G. Zhang, J. T. Sun, T. Low, L. Z. Zhang, Y. Pan, Q. Liu, J. H. Mao, H. T. Zhou, H. M. Guo, S. X. Du, F. Guinea, and H.-J. Gao, Phys. Rev. B **84**, 245436 (2011).
[39] Y. Ying, R. K. Saini, F. Liang, A. K. Sadana, and W. E. Billups, Org. Lett. **5**, 1471 (2003).

[40] S. Kyatskaya, J. R. G. Mascarós, L. Bogani, F. Hennrich, M. Kappes, W. Wernsdorfer, and M. Ruben, J. Am. Chem. Soc. **131**, 15143 (2009).

[41] L. Bogani, C. Danieli, E. Biavardi, N. Bendiab, A.-L. Barra, E. Dalcanale, W. Wernsdorfer, and A. Cornia, Angew. Chem. **121**, 760 (2009).

[42] L. Bogani and W. Wernsdorfer, Inorg. Chim. Acta **361**, 3807 (2008).

[43] H. P. Boehm, Carbon **32**, 759 (1994).

[44] L. Routaboul, P. Braunstein, J. Xiao, Z. Zhang, P. A. Dowben, G. Dalmas, V. Da Costa, O. Flix, G. Decher, L. G. Rosa, and B. Doudin, J. Am. Chem. Soc. **134**, 8494 (2012).

[45] M. Mannini, F. Pineider, P. Sainctavit, C. Danieli, E. Otero, C. Sciancalepore, A. M. Talarico, M.-A. Arrio, A. Cornia, D. Gatteschi, and R. Sessoli, Nat. Mater. **8**, 194 (2009).

[46] M. Mannini, F. Pineider, C. Danieli, F. Totti, L. Sorace, P. Sainctavit, M.-A. Arrio, E. Otero, L. Joly, J. C. Cezar, A. Cornia, and R. Sessoli, Nature (London) **468**, 417 (2010).

[47] C. F. Hirjibehedin, C.-Y. Lin, A. F. Otte, M. Ternes, C. P. Lutz, B. A. Jones, and A. J. Heinrich, Science **317**, 1199 (2007).

[48] A. Rajca, A. Olankitwanit, Y. Wang, P. J. Boratyski, M. Pink, and S. Rajca, J. Am. Chem. Soc. **135**, 18205 (2013).

[49] Y. Zhang, S. Kahle, T. Herden, C. Stroh, M. Mayor, U. Schlickum, M. Ternes, P. Wahl, and K. Kern, Nat. Commun. **4**, 2110 (2013).

[50] C. Herrmann, G. C. Solomon, and M. A. Ratner, J. Chem. Phys. **134**, 224306 (2011).

[51] O. Kahn, Science **279**, 44 (1998).

[52] M. Maesato, T. Kawashima, Y. Furushima, G. Saito, H. Kitagawa, T. Shirahata, M. Kibune, and T. Imakubo, J. Am. Chem. Soc. **134**, 17452 (2012).

[53] M. Mas-Torrent, N. Crivillers, V. Mugnaini, I. Ratera, C. Rovira, and J. Veciana, J. Mater. Chem. **19**, 1691 (2009).

[54] K. Matsuda and M. Irie, Chemistry **7**, 3466 (2001).

[55] H. Nishide, S. Iwasa, Y.-J. Pu, T. Suga, K. Nakahara, and M. Satoh, Electrochim. Acta **50**, 827 (2004).

[56] W. Choi, D. Harada, K. Oyaizu, and H. Nishide, J. Am. Chem. Soc. **133**, 19839 (2011).

[57] K. Nakahara, S. Iwasa, M. Satoh, Y. Morioka, J. Iriyama, M. Suguro, and E. Hasegawa, Chem. Phys. Lett. **359**, 351 (2002).

[58] T. Suga, H. Ohshiro, S. Sugita, K. Oyaizu, and H. Nishide, Adv. Mater. **21**, 1627 (2009).

[59] K. Oyaizu and H. Nishide, Adv. Mater. **21**, 2339 (2009).

[60] T. Suga, H. Konishi, and H. Nishide, Chem. Commun. 1730 (2007).

[61] L. Bugnon, C. J. H. Morton, P. Novak, J. Vetter, and P. Nesvadba, Chem. Mater. **19**, 2910 (2007).

[62] C. Simão, M. Mas-Torrent, N. Crivillers, V. Lloveras, J. M. Arts, P. Gorostiza, J. Veciana, and C. Rovira, Nat. Chem. **3**, 359 (2011).

[63] J. Lee, E. Lee, S. Kim, G. S. Bang, D. A. Shultz, R. D. Schmidt, M. D. E. Forbes, and H. Lee, Angew. Chem., Int. Ed. Engl. **50**, 4414 (2011).

[64] I. Ratera and J. Veciana, Chem. Soc. Rev. **41**, 303 (2012).

[65] A. Datcu, N. Roques, V. Jubera, D. Maspoch, X. Fontrodona, K. Wurst, I. Imaz, G. Mouchaham, J.-P. Sutter, C. Rovira, and J. Veciana, Chemistry **18**, 152 (2012).

[66] C. Simão, M. Mas-Torrent, J. Veciana, and C. Rovira, Nano Lett. **11**, 4382 (2011).

[67] C. Herrmann, G. C. Solomon, and M. A. Ratner, J. Am. Chem. Soc. **132**, 3682 (2010).

[68] K. Sato, M. Yano, M. Furuichi, D. Shiomi, T. Takui, K. Abe, K. Itoh, A. Higuchi, K. Katsuma, and Y. Shirota, J. Am. Chem. Soc. **119**, 6607 (1997).

[69] K. Bernot, L. Bogani, A. Caneschi, D. Gatteschi, and R. Sessoli, J. Am. Chem. Soc. **128**, 7947 (2006).

[70] K. Bernot, J. Luzon, L. Bogani, M. Etienne, C. Sangregorio, M. Shanmugam, A. Caneschi, R. Sessoli, and D. Gatteschi, J. Am. Chem. Soc. **131**, 5573 (2009).

[71] K. E. Vostrikova, Coord. Chem. Rev. **252**, 1409 (2008).

[72] C. Train, L. Norel, and M. Baumgarten, Coord. Chem. Rev. **253**, 2342 (2009).

[73] S. Haas, E. Heintze, S. Zapf, B. Gorshunov, M. Dressel, and L. Bogani, Phys. Rev. B **89**, 174409 (2014).

[74] L. Bogani, J. Appl. Phys. **109**, 07B115 (2011).

[75] M. Imada, A. Fujimori, and Y. Tokura, Rev. Mod. Phys. **70**, 1039 (1998).

[76] K. Awaga and Y. Maruyama, J. Chem. Phys. **91**, 2743 (1989).

[77] A. Rose, Phys. Rev. **97**, 1538 (1955).

[78] M. Lampert, Phys. Rev. **103**, 1648 (1956).

[79] A. A. A. Grinberg, S. Luryi, M. R. Pinto, and N. L. Schryer, IEEE Trans. Electron Devices **36**, 1162 (1989).

[80] J. A. Geurst, Phys. Status Solidi **15**, 107 (1966).

[81] A. Ioannidis, E. Forsythe, Y. Gao, M. W. Wu, and E. M. Conwell, Appl. Phys. Lett. **72**, 3038 (1998).

[82] R. W. I. de Boer and A. F. Morpurgo, Phys. Rev. B **72**, 073207 (2005).

[83] M. Stossel, J. Staudigel, F. Steuber, J. Blassing, J. Simmerer, and A. Winnacker, Appl. Phys. Lett. **76**, 115 (2000).

[84] G. Horowitz, Adv. Mater. **10**, 365 (1998).

[85] E. F. Ullman, J. H. Osiecki, D. G. B. Boocock, and R. Darcy, J. Am. Chem. Soc. **94**, 7049 (1972).

[86] A. Caneschi, D. Gatteschi, R. Sessoli, and P. Rey, Acc. Chem. Res. **22**, 392 (1989).

[87] E. T. Chernick, Q. Mi, R. F. Kelley, E. A. Weiss, B. A. Jones, T. J. Marks, M. A. Ratner, and M. R. Wasielewski, J. Am. Chem. Soc. **128**, 4356 (2006).

[88] K. Matsuda and M. Irie, J. Am. Chem. Soc. **122**, 7195 (2000).

[89] H. Komatsu, M. M. Matsushita, S. Yamamura, Y. Sugawara, K. Suzuki, and T. Sugawara, J. Am. Chem. Soc. **132**, 4528 (2010).

[90] See Supplemental Material at http://link.aps.org/supplemental/10.1103/PhysRevB.93.165201 for synthesis and structural data of the nitronyl-nitroxide radicals, further information on the statistical analysis on the transport measurements, and a Mott-insulator scaling comparison with our data.

[91] J. H. Osiecki and E. F. Ullman, J. Am. Chem. Soc. **90**, 1078 (1968).

[92] E. F. Ullman, L. Call, and J. H. Osiecki, J. Org. Chem. **35**, 3623 (1970).

[93] W. Brütting, Phys. Status Solidi **201**, 1035 (2004).

[94] M. Dressel and G. Grüner, *Electrodynamics of Solids: Optical Properties of Electrons in Matter* (Cambridge University Press, Cambridge, UK, 2002).

[95] C. Cervetti, E. Heintze, B. Gorshunov, E. Zhukova, S. Lobanov, A. Hoyer, M. Burghard, K. Kern, M. Dressel, and L. Bogani, Adv. Mater. **27**, 2676 (2015).

[96] A. Baniodeh, Y. Liang, C. E. Anson, N. Magnani, A. K. Powell, A.-N. Unterreiner, S. Seyfferle, M. Slota, M. Dressel, L. Bogani, and K. Goß, Adv. Funct. Mater. **24**, 6280 (2014).
[97] R. Smith and A. Rose, Phys. Rev. **97**, 1531 (1995).
[98] R. W. I. de Boer, J. Appl. Phys. **95**, 1196 (2004).
[99] A. D. Schricker, F. M. Davidson, R. J. Wiacek, and B. A. Korgel, Nanotechnology **17**, 2681 (2006).
[100] A. A. Talin, F. Léonard, B. S. Swartzentruber, X. Wang, and S. D. Hersee, Phys. Rev. Lett. **101**, 076802 (2008).
[101] A. M. Katzenmeyer, F. Leonard, A. A. Talin, M. E. Toimil-Molares, J. G. Cederberg, J. Y. Huang, and J. L. Lensch-Falk, IEEE Trans. Nanotechnol. **10**, 92 (1961).
[102] G. T. Wright, Solid.-State. Electron. **2**, 165 (1961).
[103] J. L. Brédas, J. P. Calbert, D. A. da Silva Filho, and J. Cornil, Proc. Natl. Acad. Sci. USA **99**, 5804 (2002).
[104] W. Kohn, A. D. Becke, and R. G. Parr, J. Phys. Chem. **100**, 12974 (1996).
[105] Y. Shao, L. F. Molnar, Y. Jung, J. Kussmann, C. Ochsenfeld, S. T. Brown, A. T. B. Gilbert, L. V. Slipchenko, S. V. Levchenko, D. P. ONeill, R. A. DiStasio, R. C. Lochan, T. Wang, G. J. O. Beran, N. A. Besley, J. M. Herbert, C. Y. Lin, T. Van Voorhis, S. H. Chien *et al.*, Phys. Chem. Chem. Phys. **8**, 3172 (2006).
[106] G. Kresse and J. Hafner, Phys. Rev. B **47**, 558 (1993).
[107] G. Kresse and J. Hafner, Phys. Rev. B **49**, 14251 (1994).
[108] G. Kresse and J. Furthmüller, Comput. Mater. Sci. **6**, 15 (1996).
[109] G. Kresse and J. Furthmüller, Phys. Rev. B **54**, 11169 (1996).
[110] G. Kresse and D. Joubert, Phys. Rev. B **59**, 1758 (1999).
[111] J. P. Perdew, K. Burke, and M. Ernzerhof, Phys. Rev. Lett. **77**, 3865 (1996).
[112] H. J. Monkhorst and J. D. Pack, Phys. Rev. B **13**, 5188 (1976).
[113] V. Coropceanu, J. Cornil, D. A. da Silva Filho, Y. Olivier, R. Silbey, and J.-L. L. Brèdas, Chem. Rev. **107**, 926 (2007).
[114] I. G. Austin and N. F. Mott, Adv. Phys. **18**, 41 (1969).
[115] N. N. Dinh, L. H. Chi, T. T. Chung Thuy, T. Q. Trung, and V.-V. Truong, J. Appl. Phys. **105**, 093518 (2009).
[116] H.-S. Woo, Y.-B. Kim, R. Czerw, D. L. Carroll, J. Ballato, and P. M. Ajayan, J. Korean Phys. Soc. **45**, 507 (2004).
[117] S. M. Sze and K. K. Ng, *Physics of Semiconductor Devices* (John Wiley & Sons, Inc., Hoboken, NJ, 2006), Vol. 3.
[118] N. Karl, Synth. Met. **133-134**, 649 (2003).
[119] P. Mark and W. Helfrich, J. Appl. Phys. **33**, 205 (1962).
[120] P. E. Burrows, Z. Shen, V. Bulovic, D. M. McCarty, S. R. Forrest, J. A. Cronin, and M. E. Thompson, J. Appl. Phys. **79**, 7991 (1997).
[121] A. J. Campbell, D. D. C. Bradley, and D. G. Lidzey, J. Appl. Phys. **82**, 6326 (1997).
[122] M. A. Lampert and P. Mark, *Current Injection in Solids* (Academic Press, New York, 1970).
[123] W. Brütting, S. Berleb, and A. G. Mückl, Org. Electron. **2**, 136 (2001).
[124] P. W. M. Blom, M. J. M. de Jong, and J. J. M. Vleggaar, Appl. Phys. Lett. **68**, 3308 (1996).
[125] J. E. Anthony, Chem. Rev. **106**, 5028 (2006).
[126] Y. Shirota and H. Kageyama, Chem. Rev. **107**, 953 (2007).
[127] B. Purushothaman, M. Bruzek, S. R. Parkin, A.-F. Miller, and J. E. Anthony, Angew. Chem. **123**, 7151 (2011).
[128] M. E. Gershenson and V. Podzorov, Rev. Mod. Phys. **78**, 973 (2006).
[129] S. A. DiBenedetto, A. Facchetti, M. A. Ratner, and T. J. Marks, Adv. Mater. **21**, 1407 (2009).
[130] V. Podzorov, E. Menard, A. Borissov, V. Kiryukhin, J. A. Rogers, and M. E. Gershenson, Phys. Rev. Lett. **93**, 086602 (2004).
[131] V. A. Dediu, L. E. Hueso, I. Bergenti, and C. Taliani, Nat. Mater. **8**, 707 (2009).
[132] V. Dediu, M. Murgia, F. C. C. Matacotta, C. Taliani, and S. Barbanera, Solid State Commun. **122**, 181 (2002).
[133] F. J. J. Wang, Z. H. H. Xiong, D. Wu, J. Shi, and Z. V. V. Vardeny, Synth. Met. **155**, 172 (2005).
[134] C. Barraud, P. Seneor, R. Mattana, S. Fusil, K. Bouzehouane, C. Deranlot, P. Graziosi, L. Hueso, I. Bergenti, V. Dediu, F. Petroff, and A. Fert, Nat. Phys. **6**, 615 (2010).
[135] Z. H. Xiong, D. Wu, Z. V. Vardeny, and J. Shi, Nature (London) **427**, 821 (2004).
[136] C. Cervetti, A. Rettori, M. G. Pini, A. Cornia, A. Repolls, F. Luis, M. Dressel, S. Rauschenbach, K. Kern, M. Burghard, and L. Bogani, Nat. Mater. **15**, 164 (2016).
[137] L. Bogani, R. Maurand, L. Marty, C. Sangregorio, C. Altavilla, and W. Wernsdorfer, J. Math. Chem. **20**, 2099 (2010).
[138] L. Bogani, in *Experiments on Molecular Magnets for Molecular Spintronics*, Structure and Bonding Series Vol. 164 (Springer, Berlin, 2014), p. 331.